

UNCLASSIFIED

Copy 6  
RM L55A05

NACA RM T.55A05

**NACA**

# RESEARCH MEMORANDUM

INVESTIGATION OF A HIGH-PERFORMANCE AXIAL-FLOW COMPRESSOR  
TRANSONIC INLET ROTOR DESIGNED FOR 37.5 POUNDS  
PER SECOND PER SQUARE FOOT OF FRONTAL AREA  
AERODYNAMIC DESIGN AND OVERALL PERFORMANCE

By Melvyn Savage and A. Richard Felix

Langley Aeronautical Laboratory  
Langley Field, Va.

**CLASSIFICATION CHANGED**

UNCLASSIFIED

To: -----

LANGLEY FIELD

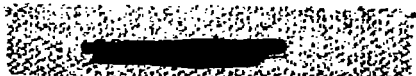
By authority of *TPA #33* CLASSIFIED DOCUMENT  
This material contains information affecting the National Defense of the United States within the meaning of the espionage laws, Title 18, U.S.C., Secs. 793 and 794, the transmission or revelation of which in any manner to an unauthorized person is prohibited by law. *10-25-60*  
*ERK*

**NATIONAL ADVISORY COMMITTEE  
FOR AERONAUTICS**

WASHINGTON  
March 24, 1955

~~CONFIDENTIAL~~

UNCLASSIFIED


  
 NATIONAL ADVISORY COMMITTEE FOR AERONAUTICS

 RESEARCH MEMORANDUM
   


UNCLASSIFIED

## INVESTIGATION OF A HIGH-PERFORMANCE AXIAL-FLOW COMPRESSOR

## TRANSONIC INLET ROTOR DESIGNED FOR 37.5 POUNDS

## PER SECOND PER SQUARE FOOT OF FRONTAL AREA

## AERODYNAMIC DESIGN AND OVERALL PERFORMANCE

By Melvyn Savage and A. Richard Felix

## SUMMARY

The present investigation includes the design and tests of a **transonic** inlet rotor in which emphasis was placed on increasing the design specific weight flow (SWF) while maintaining reasonably high pressure ratio and efficiency. The design air SWF was **37.5 lb/sec/sq ft** frontal area. The rotor has a 12-inch tip diameter and an inlet hub-tip ratio of **0.35** and was designed for no inlet guide vanes. The mass-weighted design pressure ratio is **1.293**; the design tip speed is **972 ft/sec**; and the design inlet axial Mach number is **0.628**. This paper presents the overall performance as obtained from detailed surveys taken downstream of the rotor which was tested in Freon.

At design speed a peak efficiency of **0.92** was obtained at an SWF of **35.5 lb/sec/sq ft** and a mass-weighted pressure ratio of **1.28**. At design SWF (**37.5 lb/sec/sq ft**) the efficiency was about **0.87** and the pressure ratio was **1.23** compared with **1.263**, which is approximately the Freon pressure ratio corresponding to the air design value of **1.293**. Peak efficiency gradually decreased from **0.92** at design speed to **0.85** at 121 percent design where SWF was **38.0 lb/sec/sq ft** and the mass-weighted pressure ratio was **1.425**. The maximum SWF obtained at 1.21 percent of design speed was **40.0 lb/sec/sq ft** which corresponds to an inlet axial Mach number of slightly over **0.70** and about **92** percent of the theoretical maximum flow capacity at a hub-tip ratio of **0.35**.


  
 UNCLASSIFIED

## INTRODUCTION

For high-speed flight, it is desirable to keep the turbojet-engine frontal area to a minimum. Since engine thrust is proportional to the weight flow passing through the engine, high-thrust engines will require that the maximum flow possible be crammed through an engine of given diameter. The flow-handling capacity of the compressor has been one of the limiting factors in the development of high-thrust engines. Then too, since it is desirable to maintain a high engine thrust-weight ratio, multistage axial-flow compressors should be designed for the highest practical values of stage pressure ratio and weight flow per square foot of frontal area (specific weight flow, SWF) because these parameters directly affect compressor size and weight. Specific weight flow can be increased by either decreasing the hub-tip ratio or increasing the inlet axial velocity, or both. It has already been shown that efficient performance is possible for high-pressure-ratio stages in which the blade sections are operating at transonic relative inlet Mach numbers. (See refs. 1, 2, and 3.) It has also been shown that efficient transonic rotors at hub-tip ratios as low as 0.4 with a specific weight flow of 34.9 lb/sec/sq ft frontal area can be designed (ref. 3).

The present investigation includes the design and tests of a transonic inlet rotor in which emphasis was placed on increasing the level of design specific weight flow while maintaining a reasonably high pressure ratio and efficiency. The design air SWF without correction for boundary-layer blockage in the inlet was 37.5 lb/sec/sq ft frontal area. All design parameters were selected with the intention that the rotor should be capable of passing higher than design specific flows with reasonable efficiency. The rotor has a 12-inch tip diameter and an inlet hub-tip ratio of 0.35 and was designed for no inlet guide vanes. The mass-weighted design pressure ratio is 1.295; the design tip speed is 972 ft/sec; and the design inlet axial Mach number is 0.628. All blade-section selections were made by utilizing the low-speed cascade data of references 4 and 5. The blade mean-line type was varied from hub to tip.

The speed of sound in Freon-12 is about 45 percent of that in air. Therefore, the duplication of the air Mach numbers in the Freon tests requires less than half the rotational speed needed in air tests. The blade stress levels are thus reduced sufficiently to permit quick fabrication of blades from fiber glass and a polyester resin. A description of the rotor and blade fabrication is presented in the appendix. The rotor was tested in Freon-12 in a supersonic compressor test stand at the Langley Aeronautical Laboratory.

A	frontal area, sq ft
$C_{l_0}$	camber, expressed as design lift coefficient of isolated airfoil
c	blade chord, ft
$c_{pm}$	specific heat at constant pressure obtained by using average of <u>upstream</u> and downstream temperatures at each radial station
D	diffusion factor, $D = 1 - \frac{V_{2R}}{V_{1R}} + \frac{\Delta V_T}{2\sigma V_{1R}}$
M	Mach number
N	rotor speed, rpm
P	static <u>pressure</u> , lb/sq ft
P	total pressure, lb/sq ft
q	<u>dynamic pressure</u> , lb/sq ft
r	radius, ft
$R_{LE}$	leading-edge radius, percent chord
$R_{TE}$	trailing-edge radius, percent chord
SWF	specific weight flow, $\frac{W\sqrt{\theta}}{\delta A}$ , lb/sec/sq ft frontal area
t	blade maximum thickness, ft
T	total temperature, 'R
AT	total <u>temperature</u> rise, 'R
U	blade speed, ft/sec
V	<u>velocity</u> , ft/sec
W	weight flow, lb/see

$\alpha$	angle between flow direction <b>and</b> blade chord, deg
$\beta$	<b>angle</b> between flow direction <b>and</b> axial direction, deg
$\delta$	<b>ratio</b> of <b>inlet total</b> pressure to <b>NACA</b> standard sea-level pressure
$\eta_m$	efficiency based on momentum
$e$	<b>ratio</b> of <b>inlet total</b> temperature to <b>NACA</b> standard <b>sea-level</b> temperature
$\theta_o$	flow turning angle, deg
$\rho$	mass density, <b>slugs/ft<sup>3</sup></b>
$\sigma$	solidity
$\xi$	blade-setting <b>angle</b> , angle between blade chord and rotor axis, deg

**Subscripts:**

A	air
<b>a</b>	<b>axial</b>
d	design
F	<b>Freon</b>
h	hub
R	relative to rotor blade
t	t i p
T	tangential
v	venturi
1	<b>upstream</b> of rotor
2	downstream of rotor

## ROTOR DESIGN

## General

The rotor design generally consists of two phases, that is, the calculation of **velocity diagrams** from prescribed design flow and pressure-ratio conditions and the selection of **blading** to fit the **velocity-diagram** conditions. Actually, the **blading performance** must be considered in the **selection** of velocity diagrams to ensure good performance. It is consideration of blade **performance** which dictates the levels of **Mach** number, pressure ratio, and inlet **angle** that can be used in the **computation** of the **velocity diagrams**.

Figure 1 shows the variation of tip inlet **Mach** number relative to the rotor with specific weight flow for various hub inlet angles at  $r_h/r_t = 0.35$  for no-guide-vane conditions (axial inlet flow). The combination of low hub inlet angles as shown in figure 1 and the thickness of the hub sections required for structural reasons presents a blade-passage choking problem, at least on a two-dimensional basis. Choking in the blade passage may be relieved by using higher inlet angles (higher rotational speed) but, as can be seen in figure 1, higher hub inlet angles are associated with higher tip inlet **Mach** numbers. Hence, a compromise between high inlet **Mach** number conditions at the tip and choke conditions and the resulting high blade surface **Mach** numbers at the hub section must be reached. A relative tip **Mach** number of 1.1 was selected for this design. This value should not be construed to be a limiting value for efficient performance. It appeared to be a value which should ensure good performance on the basis of references 1, 2, 3, and 6. At the design specific weight flow of 37.5 lb/sec/sq ft of frontal area, the resulting hub inlet angle was 26.7° at a relative inlet **Mach** number of 0.70. Some unpublished high-speed cascade tests at similar conditions have indicated that, on a two-dimensional basis, inlet relative **Mach** numbers as high as 0.80 should be possible. Hence, even on a two-dimensional basis the hub should be capable of an increase over the design specific weight flow of some 7 to 8 percent. The sections outboard of the hub section present a more open blade passage and, consequently, the choking problem is much less severe and, in fact, generally does not exist. Therefore, when the hub section is two dimensionally choked the streamlines can be displaced around the hub region. Since the amount of this three-dimensional movement is quite small, it is likely that somewhat higher flows than occur when the hub section is choked two dimensionally can be obtained without seriously affecting the rotor discharge angles and flow distribution.

### Velocity Diagrams

The design total-pressure ratio varied from 1.25 at the hub to 1.35 at the tip. Moderate rather than high pressure ratios were designed for since the main emphasis in the design of this rotor was high specific weight flow. The radial variation in design pressure ratio was selected so as to keep the Mach number and flow angle leaving the rotor hub in stator coordinates to lower values than would be possible for a constant pressure ratio of 1.293, which is the mass-weighted design pressure ratio. Again, it must be emphasized that these pressure ratios are not absolute design limits but were selected because they appeared to be in the high efficiency range. The use of higher design pressure ratios would reduce the loading margin available for overspeed tests as well as raise the stator inlet Mach numbers, which is less significant.

The velocity diagrams were computed by satisfying the conditions of simple radial equilibrium  $\frac{1}{\rho} \frac{dp}{dr} = \frac{V_{\theta}^2}{r}$ . The computations were made at radii bounding four stream tubes of equal weight flows. This required some iterative calculation but it was found that dividing both upstream and downstream annuli into equal-area sections was fairly close as a first approximation in the iterative procedure. The inner-casing radius was increased to  $r_h/r_t = 0.45$  at the rotor discharge. No boundary-layer allowance was added and a rotor polytropic efficiency of 0.90 was assumed for the calculation. Figure 2 presents the design velocity-diagram data.

### Blade Selection

The transonic compressor results to date have indicated that efficient blade section performance at high relative inlet Mach numbers may be obtained by keeping the level of blade surface Mach numbers as low as possible. This was done in reference 1 by using blades made up of the NACA 65-series thickness distribution and the NACA A<sub>2</sub>I<sub>8</sub>b mean line which moved the loading toward the rearward portion of the blade where the average velocities are less. It was also done in references 2 and 3 by reducing the thickness in the forward portion of the blade while at the same time reducing the blade maximum thickness. Both of these methods of holding blade surface Mach numbers down appeared to be desirable. It was felt that more nearly optimum transmit blade sections could be designed by combining the desirable features of each.

Thickness distribution.- It is believed that transonic sections should be thin in the forward portion with very little surface curvature. As a result, surface Mach numbers would be reduced and, for inlet Mach numbers high enough for a supersonic region to exist on the suction surface, the strength of the shock emanating from the suction surface

would be reduced and the likelihood of flow separation would thus be reduced. Hence, the 65-percent-chord point was selected as the Point of maximum thickness as compared with the 40-percent-chord point for the NACA 65-series thickness distribution commonly used in subsonic compressor blading. In developing a 10-percent-thick section, the Y-ordinate at 5-percent chord was arbitrarily fixed at 1.53 percent. The first 5 percent of the blade is the 7.1-percent-thick NACA 65-series thickness distribution which matches the fixed 5-percent-chord ordinate value of 1.53. From 5 percent to 65 percent of the chord, a faired curve was drawn to provide a smooth transition from the derived 5 percent of nose region to the 65-percent point while at the same time attempting to keep surface curvature low. The rearward portion of the thickness distribution was obtained by fairing between the 65-percent point and a 1-percent-chord trailing-edge radius, again trying to maintain low surface curvature. The coordinates for this thickness distribution, herein referred to as the T1 thickness distribution, are presented for 10-percent maximum thickness in table I and a comparison with the 65-series thickness distribution is presented in figure 3(a). The vertical scale has been expanded to emphasize the difference between the two thickness distributions. Since thin sections will have lower surface Mach numbers, the rotor-blade-section maximum thickness was reduced as much as structural considerations would allow. As a result, blade maximum thickness varied from 8 percent to 4 percent of the chord from hub to tip. The variation of leading-edge and trailing-edge radii with maximum thickness is indicated in figure 3(b).

Wan-line shape. - Since the tip section has the highest inlet Mach numbers, the tip mean line selected was that having the greatest rearward shift in loading, that is, the NACA A<sub>2</sub>I<sub>8b</sub> mean line. (Mean-line designations are explained in ref. 7.) Because of the combination of low inlet angle and high solidity at the hub section and the need for sufficient hub thickness from structural considerations, the hub problem is one of avoiding a choked passage, at least on a two-dimensional basis. For low-inlet-angle high-solidity conditions the NACA A<sub>10</sub> mean line presents a considerably more open passage than the NACA A<sub>2</sub>I<sub>8b</sub> mean line when 65-series thickness distributions are used. (For example, see ref. 4.) When the T1 thickness distribution is used with these mean lines, the blade with the NACA A<sub>10</sub> mean line still presents a considerably more open passage than the NACA A<sub>2</sub>I<sub>8b</sub>. However, the A<sub>6</sub>I<sub>4b</sub> and the A<sub>10</sub> blades had identical minimum passage areas at design angle of attack. Hence, the question of which of the two blades would be the better for a transonic rotor-hub condition cannot be answered on a minimum-passage-area basis alone. Some unpublished high-speed cascade test results for the T1(18A<sub>6</sub>I<sub>4b</sub>)08 blade at conditions similar to the hub conditions in this rotor indicated a fairly severe second velocity peak in the rearward portion of the blade where the thickened boundary layer will reduce the amount of diffusion that may be tolerated without flow separation.

Therefore, to reduce this peak it was decided to utilize the NACA A<sub>10</sub> mean line, which has less curvature in the rearward portion, for the rotor hub-section. The blade sections for the intermediate-three radial stations had a gradual change in mean-line loading from the A<sub>10</sub> to the A<sub>2I8b</sub>. The middle station of the blade had an A<sub>6I4b</sub> mean line and each of the other two had mean-line shapes midway between those of the two adjacent radial stations. This selection of mean-line shape at each radial station should not be construed to mean that these are the optimum blades for that particular station. For example, it is not obvious that the A<sub>6I4b</sub> mean line selected for the middle radial station is any more effective than the A<sub>2I8b</sub> mean line. It was reasoned that the A<sub>6I4b</sub> could be used since the operating inlet Mach number level of that station was considerably below that of the tip, where the A<sub>2I8b</sub> blade was used. A linear progression of mean-line types from hub to tip was used to promote the likelihood of smoothly faired blades.

Blade camber, solidity, and setting-angle selection.- All velocity diagrams were converted to equivalent constant axial-velocity conditions by maintaining all tangential components and averaging upstream and downstream axial velocities at each streamline. The resulting diagrams were used both for selection of blade camber and blade-setting angle. The selection of blade solidities requires a compromise between aerodynamic requirements at the hub and tip and blade stress limitations. As design solidity is decreased, camber must be increased for the same turning angle. At transonic inlet relative Mach numbers of the order of 1.1, definite limits regarding the blade surface curvature and blade surface Mach numbers have not been established. Hence, all that can be stated is that it is desirable to keep blade surface curvature low and, hence, solidity as high as possible in the tip region.

For low hub-tip ratios ( $r_h/r_t$  of the order of 0.35) the selection of high tip solidity and constant-chord blades will result in high hub solidities. For example, a value of  $\sigma_t = 0.75$  at  $r_h/r_t = 0.35$  will result in  $\sigma_h = 2.14$ . Since the minimum passage area between blades is decreased with increasing solidity, high hub solidity can result in a two-dimensionally choked passage. However, if hub solidity is decreased, then camber will increase and, although no choked passage occurs, surface Mach numbers become excessive because of large blade surface curvature. Definite limits have not been established regarding either how nearly choked, on a two-dimensional basis, the hub section can be or how high the hub camber can be before surface Mach numbers become excessive and poor performance results. Aside from aerodynamic requirements on blade-chord variations, any severe increase in chord with radius would result in high blade stresses. Therefore, the selection of blade solidities resolves itself into a compromise of stress and aerodynamic considerations with the limits on both not well defined.

The increase in chord from hub to tip was arbitrarily chosen to be approximately 20 percent to provide a reasonably strong blade. Once the variation in chord from hub to tip is fixed, the selection of solidity at any radial station defines the solidity all along the blade. The hub solidity was chosen as 1.5 and as a result the tip solidity was 0.75. This selection was an attempt to arrive at an effective compromise between the aerodynamic requirements of the hub and tip and provided a margin of 7 to 8 percent between minimum passage area and choke flow area at the hub. The resulting tip camber was 0.70.

The blade camber and blade-setting angles were determined from the low-speed cascade data presented in references k and 5. In reference k it was shown that at the design angle of attack all the  $C_{l_0} = 1.2$  mean lines investigated produce approximately the same turning angle and that the design angle of attack varies almost linearly with variation in mean-line loading distribution. Hence, the more extensive cascade data of reference 5 could be used to obtain the appropriate cambers for conditions at which the other mean lines were not tested. Suitable adjustment of angle of attack was necessary to account for the change in design angle of attack with variation in loading distribution. Linear interpolations were used to obtain all intermediate mean-line conditions.

The results obtained in reference 1 indicated that in the transonic speed range the angle of attack associated with peak efficiency was some  $4^\circ$  above the low-speed design angle of attack. In order to produce a given turning angle when operating above low-speed design angle of attack, it is necessary to use a lower camber than would be prescribed by the low-speed design charts. Therefore, both design and off-design low-speed cascade data were used to determine the cambers and angles of attack which result for blade sections operating from  $2.4^\circ$  at the hub to  $3.2^\circ$  at the tip above their design angles of attack as indicated from low-speed cascade tests.

Details of the design blading used are presented in figure 4. It should be noted that blade sections and angles were all determined in the planes indicated by the capital letters. In computing the solidity the mean radii between corresponding inlet and outlet radii were used. A photograph of the rotor is shown as figure 5.

## COMPRESSOR INSTALLATION AND TEST PROCEDURE

### Test Rig

The compressor installation used in these tests is a closed-circuit rig equipped to use either Freon or air as a testing medium. A schematic diagram of the layout is shown in figure 6(a). This installation is

~~CONFIDENTIAL~~

essentially the same as the one described in reference 8 except that the 1,000-hp compressor drive motor has been replaced by a 3,000-hp induction motor which, with a gear ratio of 2.015 to 1, makes possible a top rotor speed of 13,300 rpm. Since it is difficult to increase the flow area at the inlet to the radial diffuser, low-hub-tip-ratio high-flow rotors could only be tested by reducing the rotor tip diameter to eliminate the problem of a choked diffuser inlet. Hence, the tip diameter of the test section was reduced from 16 inches to 12 inches. This reduction in rotor size and actual volume flow would also reduce the pressure loss in the system, which is important because there is no auxiliary boost. To reduce further the pressure loss of the system, one of the 60 mesh screens upstream of the venturi meter was removed. A schematic of the test section is indicated in figure 6(b).

### Test Procedure

The rotor tests were made over a range of corrected tip speeds from 81 to 121 percent of the design speed. At each speed the weight flow was varied from the maximum possible to the surge point by continuously increasing the back pressure. The settling-chamber pressure was held constant at approximately 20 inches of mercury absolute.

The tests were conducted by using freon-~ as a testing medium. At the design inlet axial Mach number of 0.628 the Freon equivalent corrected tip speed corresponding to the design air value of 972 ft/sec was 437 ft/sec. This equivalent condition is the rotor speed in Freon at which both inlet axial Mach number and mean radius inlet angle are the same as the design air values. (See ref. 9.) The Freon equivalent pressure ratio corresponding to the air design value of 1.293 is 1.263.

### Instrumentation and Data Reduction

Flow conditions upstream of the rotor were obtained by measuring stagnation pressure and temperature in the settling chamber and using four inner- and outer-wall static taps circumferentially located at 90° intervals approximately 1.5 inches upstream of the rotor. The following measurements were made approximately 1.5 inches do-stream of the rotor:

(1) Total temperatures were obtained by using two rakes of four shielded chromel-alumel thermocouples spaced radially to cover the entire passage and located circumferentially approximately 180° apart. Figure 7(a) shows one of these rakes. These rakes were connected to a four-bell rake upstream to read the temperature differential across the rotor at various radial stations.

(2) Radial surveys at 13 points of **total** and static pressure and flow **angle** were made by using a prism probe of the **type** described in reference 10 and shown in figure 7(b).

(3) Wall static pressures were obtained from four **inner-** and **outer-** wall static taps located at 90° **intervals**.

The survey data in conjunction with the wall-tap and the upstream instrumentation readings were used to **compute** mass-weighted efficiency based on the power input obtained from **momentum** considerations:

$$\eta_m = \frac{\int_{r_h}^{r_t} c_{pm} \Delta T_{isen} \rho_2 V_{a_2} dr^2}{\int_{r_h}^{r_t} U_2 V_{T_2} \rho_2 V_{a_2} dr^2}$$

where

$$\Delta T_{isen} = \left[ \left( \frac{P_2}{P_1} \right)^{\frac{\gamma-1}{\gamma}} - 1 \right] T_1$$

This equation **presumes** that there is no **inlet** swirl; **however, some** unpublished results of a **preliminary** detailed survey upstream of the rotor **indicate** that there is a small amount of swirl (**of** the order of 3°) in the direction of rotation in the **extreme** tip region. **Because** of the direction of the swirl, **the** efficiencies herein reported are **slightly** lower than would occur **if** the swirl were **taken** into account. **Only** momentum efficiencies are presented since the **small temperature rises** associated with testing in **Freon** at these pressure **ratios** make **it** difficult to obtain accurate **temperature-measured** efficiencies.

Mass-weighted overall **pressure** ratio was obtained using the **following** equation:

$$\frac{P_2}{P_1} = \frac{\int_{r_h}^{r_t} \frac{P_2}{P_1} \rho_2 V_{a_2} dr^2}{\int_{r_h}^{r_t} \rho_2 V_{a_2} dr^2}$$

Weight flow was obtained by utilizing the previously **mentioned** **upstream** measurements. No blockage factor was included **in** the area

term of the continuity equation since the inlet contraction ratio and Reynolds number were in the range in which, within the weight-flow-measuring accuracy, the flow coefficient may be considered to be unity. A preliminary examination of the inlet total-pressure distribution obtained from single line traverses made upstream of the rotor further corroborated this assumption. There was some radial variation in static pressure at the inlet and an average of the inner- and outer-wall tap readings was used. Weight flow was also computed by using the downstream survey data. Figure 8(a) indicates the magnitude of the difference between the upstream and downstream measured weight flows. Generally, the agreement between  $W_1$  and  $W_2$  was within  $\pm 2\frac{1}{2}$  percent. A calibrated venturi indicated in figure 6 was also used to compute weight flow. The variation between the venturi weight flow and the upstream weight flow is shown in figure 8(b). The venturi weight flow was generally some 2 percent greater than  $W_1$ . The weight flow used to present the overall performance is the weight flow obtained from upstream flow measurements  $W_1$ .

#### DISCUSSION OF OVERALL PERFORMANCE RESULTS

The mass-weighted overall performance of the transonic compressor rotor is presented in figure 9 where adiabatic momentum efficiency  $\eta_m$  and total-pressure ratio  $P_2/P_1$  are plotted against corrected Freon weight flow  $\frac{W_F \sqrt{\theta}}{\delta}$  for each of the rotor speeds tested. The air equivalent corrected specific weight flows which correspond to the inlet axial Mach numbers obtained in Freon are also indicated. At design speed a peak efficiency of 0.92 was obtained at 35.5 lb/sec/sq ft frontal area and a pressure ratio of 1.28. At design SWF (37.5 lb/sec/sq ft frontal area) the efficiency was about 0.87 and the pressure ratio was 1.23 compared with 1.263, which is approximately the freon pressure ratio corresponding to an air design value of 1.293. This lower than design pressure ratio results because (1) lower than design efficiency was obtained and (2) a preliminary examination of the survey data indicates lower than design turning angles over an extensive portion of the hub region and to a lesser extent at the tip region.

At and below the design speed the complete high efficiency ranges could not be obtained because the high-flow region is limited by the losses in the test loop as compared with the compressor pressure ratio since the test compressor supplied all the pumping action. The 2-percent drop in peak efficiency which occurred between design speed and 81 percent of design speed might be caused by a Reynolds number effect.

Peak efficiency gradually decreased from 0.92 at design speed to 0.84 at 121 percent design where SWF was about 38.0 lb/sec/sq ft frontal area and the pressure ratio was 1.425. The maximum SWF obtained at 121 percent of design speed was 40.0 lb/sec/sq ft frontal area which corresponds to an inlet axial Mach number of slightly over 0.7 and about 92 percent of the theoretical maximum flow capacity at a hub-tip ratio of 0.35.

#### SUMMARY OF RESULTS

The following overall performance results were obtained from an experimental investigation of a high-performance transonic axial-flow compressor rotor:

1. At design speed a peak efficiency of 0.92 was obtained at 37.5 lb/sec/sq ft frontal area and a mass-weighted pressure ratio of 1.28. At design specific weight flow (37.5 lb/sec/sq ft frontal area) the efficiency was about 0.87 and the pressure ratio was 1.23.

2. Peak efficiency gradually decreased from 0.92 at design speed to 0.84 at 121 percent design where the specific weight flow was 38.0 lb/sec/sq ft frontal area and the mass-weighted pressure ratio was 1.425.

3. The maximum flow obtained at 121 percent of design speed was 40.0 lb/sec/sq ft frontal area which corresponds to an inlet axial Mach number of slightly over 0.70 and about 92 percent of the theoretical maximum flow capacity at a hub-tip ratio of 0.35.

Langley Aeronautical Laboratory,  
National Advisory Committee for Aeronautics,  
Langley Field, Va., December 29, 1954.

## APPENDIX

## DESCRIPTION OF ROTOR FABRICATION

The materials and type of construction used in the fabrication of this rotor were unusual enough to warrant description. The rotor is of integral construction, that is, the blades and hub were built as a unit. The materials used were fiber glass, polyester resin, and balsa.

Construction of the blades was begun by building a master blade from which a mold was cast in two halves. Two types of fiber glass, roving and woven, were used in the blades, along with the polyester resin. The roving fiber glass was laid spanwise in the blade to provide tensile strength whereas the woven fiber glass was placed near the surface of the blade to supply torsional stiffness. It was found that 100 strands of roving fiber glass (approximately 1/16 inch in diameter) would provide the desired ratio of fiber glass to resin which is 7 to 3. Eight groups of 100 strands of roving fiber glass approximately 8 inches long were then assembled. On one end of each of these groups a blade was cast in the following manner. A sheet of 0.004-inch woven fiber glass was placed in each half of the mold which had been previously treated with a parting agent. Next, a sheet of 0.009-inch unidirectional woven fiber glass was placed on each half-mold such that the greater number of strands ran in the chordwise direction. The more finely woven 0.004 cloth was placed nearer the surface of the blade than the 0.009 cloth because this arrangement gives a smoother cast surface. Then one end of each of the groups of roving fiber glass was saturated in a vat of resin after which the saturated group was placed in the mold under some tension and the mold closed. After the excess resin had drained from the blade area of the mold by means of channels provided at the leading and trailing edges, the blade was allowed to cure in the mold at room temperature for several hours.

A balsa hub was turned slightly undersize to allow for a surface layer of woven fiber glass. A large center hole was drilled through the hub and slots through the outer surface into the center hole were provided for each of the eight blades. This hub was then wrapped with woven fiber glass saturated with resin and turned to the finished dimensions. The eight blades were fitted into the hub with the roving from diametrically opposite blades combed together. The roving from each diametrically opposite pair was intermeshed in the center with that of all other pairs. The center of the hub was then filled with resin and a fiber-glass filler. After the completed rotor had been allowed to cure for a considerable length of time, the rotor blades were tipped to the proper diameter.

The weight of each of the **blades with** the **protruding** roving fiber glass was 0.16 **pound**. The weight of the **hub** before any of the **blades** were inserted was 0.66 pound. The total weight of the finished rotor was **2.81 pounds**.

## REFERENCES

1. Savage, Melvyn, Erwin, John R., and Whitley, Robert P. : Investigation of an Axial-Flow Compressor Rotor Having NACA High-Speed Blade Sections (A2I8b Series) at Mean Radius Relative Inlet Mach Numbers up to 1.13. NACA RM L53G02, 1953.
2. Lieblein, Seymour, Lewis, George W., Jr., and Sandercock, Donald M. : Experimental Investigation of an Axial-Flow Compressor Inlet Stage Operating at Transonic Relative Inlet Mach Numbers. I - Over-All Performance of Stage With Transonic Rotor and Subsonic Stators Up to Rotor Relative Inlet Mach Number of 1.1. NACA RM E52A24, 1952.
3. Serovy, George K., Robbins, William H., and Glaser, Frederick W. : Experimental Investigation of a 0.4 Hub-Tip Diameter Ratio Axial-Flow Compressor Inlet Stage at Transonic Inlet Relative Mach Numbers. I - Rotor Design and Over-All Performance at Tip Speeds From 60 to 100 percent of Design. NACA RM E53I11, 1953.
4. Erwin, John R., Savage, Melvyn, and Emery, James C. : Two-Dimensional Low-Speed Cascade Investigation of NACA Compressor Blade Sections Having a Systematic Variation in Mean-Line Loading. NACA RM L53I30b, 1953.
5. Herrig, L. Joseph, Emery, James C., and Erwin, John R. : systematic Two-Dimensional Cascade Tests of NACA 65-Series Compressor Blades at Low Speeds. NACA RM L51G31, 1951.
6. Schwenk, Francis C., Lieblein, Seymour, and Lewis, George W., Jr. : Experimental Investigation of an Axial-Flow Compressor Inlet Stage Operating at Transonic Relative Inlet Mach Numbers. III - Blade-Row Performance of Stage With Transonic Rotor and Subsonic Stator at Corrected Tip Speeds of 800 and 1000 Feet Per Second. NACA RM E53G17, 1953.
7. Erwin, John R., and Yacobi, Laura A. : Method of Estimating the Incompressible-Flow Pressure Distribution of Compressor Blade Sections at Design Angle of Attack. NACA RM L53F17, 1953.
8. Goldberg, Theodore J., Boxer, Emanuel, and Bernet, Peter T. : Experimental Investigation of an Axial-Flow Supersonic Compressor Having Rounded Leading-Edge Blades With an 8-percent Mean Thickness-Chord Ratio. NACARM L53G16, 1953.
9. Boxer, Emanuel, and Erwin, John R. : Investigation of a Shrouded and an Unshrouded Axial-Flow Supersonic Compressor. NACA RM L50G05, 1950.

10. Schulze, Wallace M., Ashby, George C., Jr., and Erwin, John R. :  
Several **Combination** Probes for **Surveying** Static and **Total** Pressure  
and Flow Direction. NACA TN 2830, 1952.

TABLE I

COORDINATES FOR TL THICKNESS DISTRIBUTION

HAVING 10-PERCENT MAXIMUM THICKNESS

[Stations and ordinates in percent chord]

x	y	
	Upper surface	Lower surface
0	0	0
.500	.555	-.555
.750	.671	-.671
<b>1.250</b>	<b>.839</b>	<b>-.839</b>
2.500	1.117	-1.117
<b>5.000</b>	1.530	-1.530
<b>7.500</b>	1.830	-1.830
<b>10.000</b>	2.000	-2.080
<b>15.000</b>	<b>2.500</b>	-2.500
<b>20.000</b>	<b>2.880</b>	-2.880
<b>25.000</b>	<b>3.230</b>	-3.230
<b>30.000</b>	3.530	-3.530
<b>35.000</b>	<b>3.810</b>	-3.810
<b>40.000</b>	<b>4.050</b>	-4.050
<b>45.000</b>	4.280	-4.280
<b>50.000</b>	<b>4.510</b>	-4.510
55.000	4.730	-4.730
60.000	4.940	-4.940
<b>65.000</b>	<b>5.000</b>	-5.000
<b>70.000</b>	<b>4.870</b>	-4.870
75.000	4.570	-4.570
80.000	4.120	-4.120
<b>83.000</b>	<b>3.470</b>	-3.470
<b>90.000</b>	<b>2.710</b>	-2.710
<b>95.000</b>	1.830	-1.830
<b>100.000</b>	0	0
Leading-edge radius = 0.343 Trailing-edge radius = 1.000		

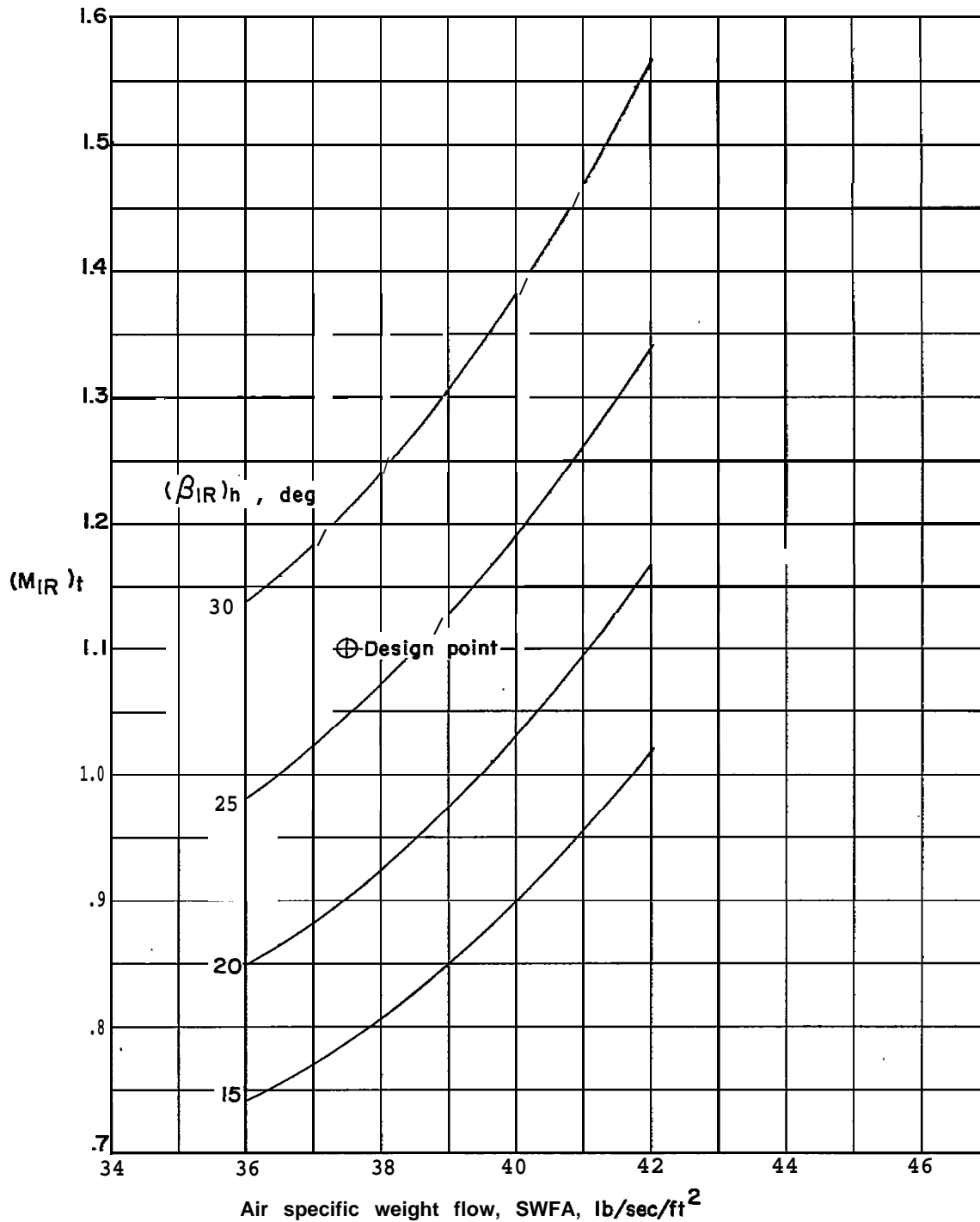
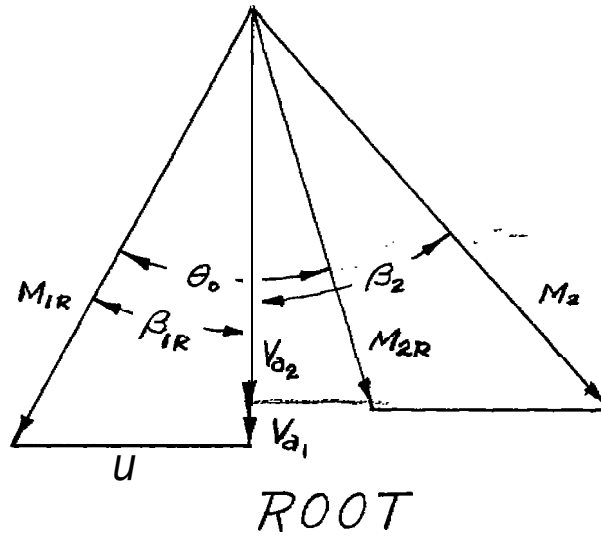
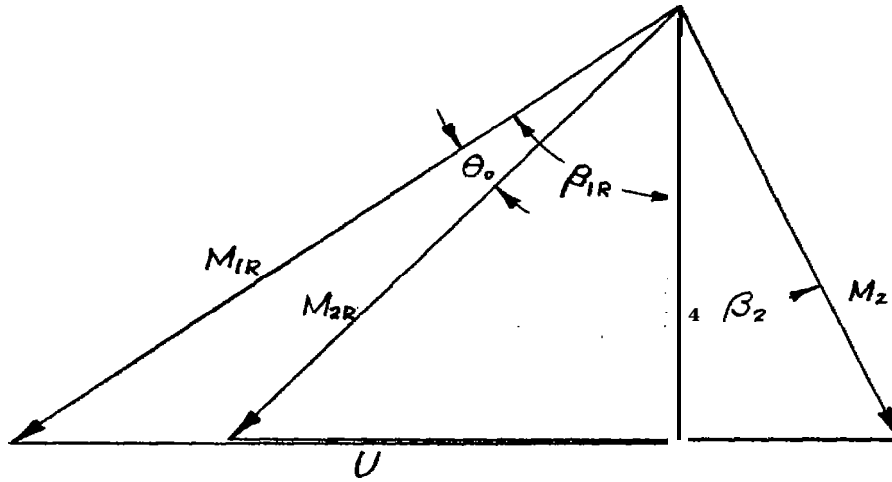


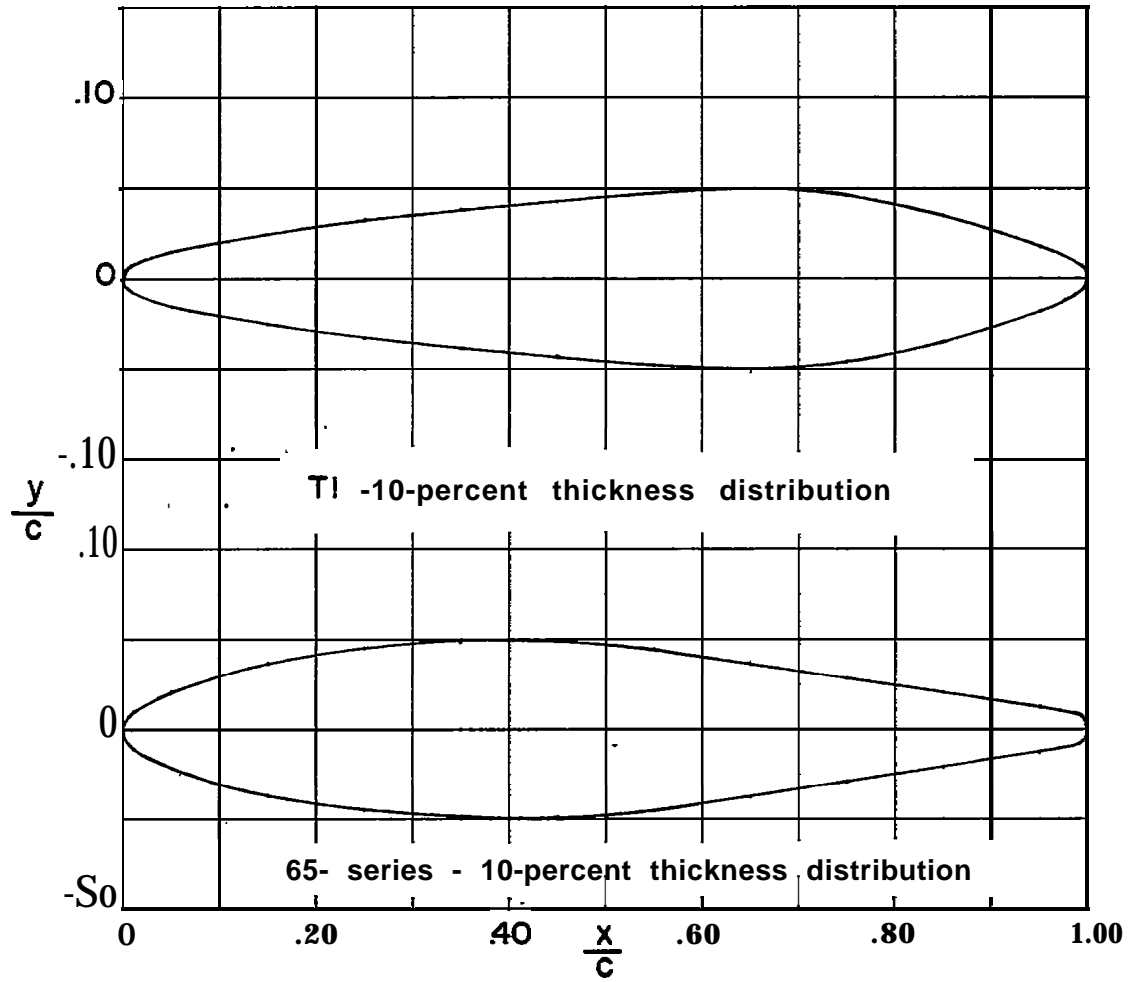
Figure 1.- Effect of air specific weight flow on rotor inlet tip Mach number for various rotor-hub inlet angles with an inlet hub-tip ratio of 0.35 and no guide vanes.



Velocity-Diagram Data

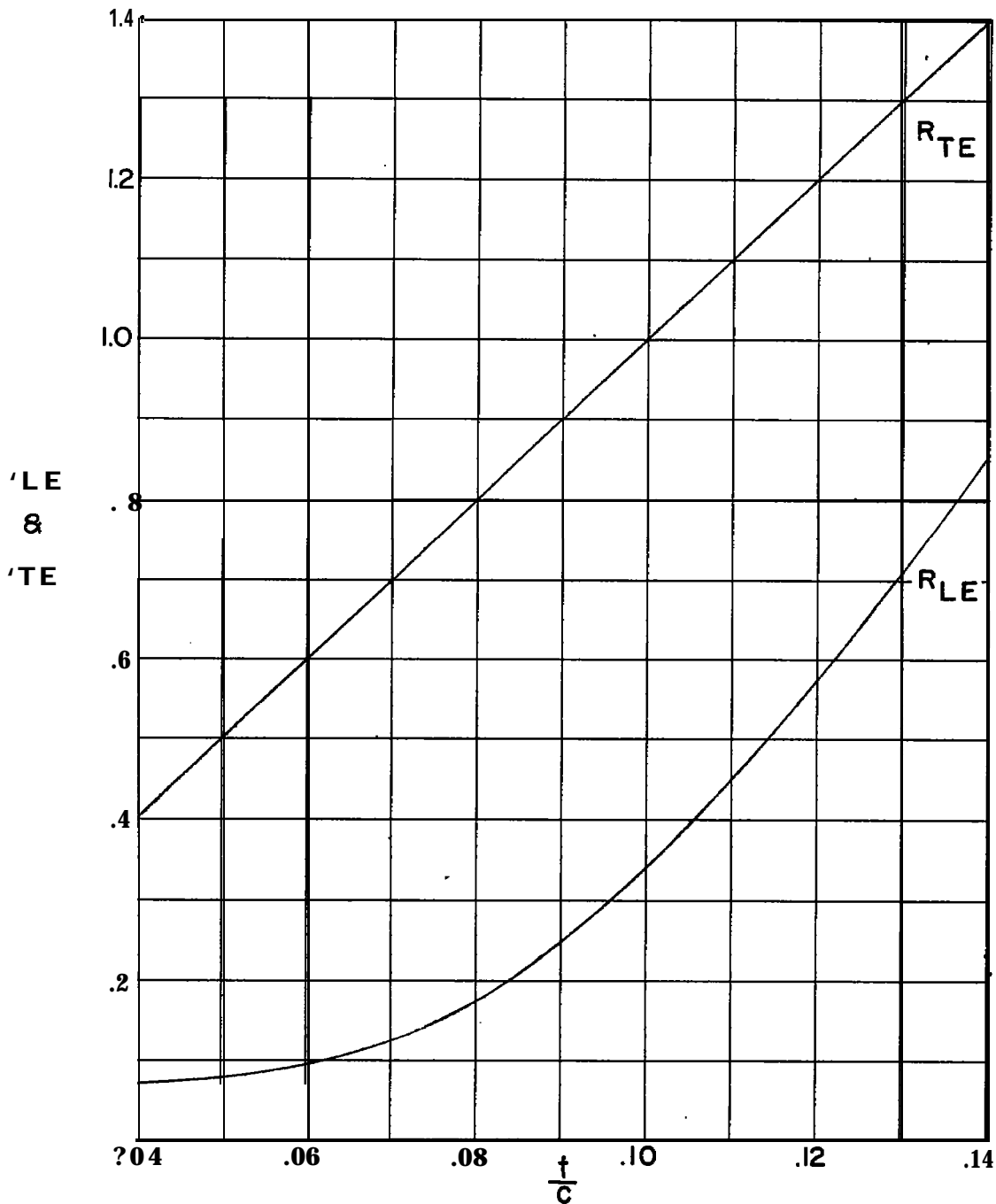
$\frac{r_1}{r_t}$	$\frac{r_2}{r_t}$	$\frac{P_2}{P_1}$	$M_{1R}$	$\beta_{1R}$ , deg	$\theta_0$ , deg	D	$\frac{\Delta p}{q_{1R}}$	$\frac{V_{a2}}{V_{a1}}$	$\beta_2$ , deg	$M_2$
0.350	0.450	1.250	0.70	26.7	34.7	0.41	0.35	0.92	40.3	0.74
.585	.646	1.275	.82	40.1	20.3	.47	.49	.92	33.1	.66
.750	.787	1.300	.93	47.2	14.2	.44	.47	.94	29.3	.65
.883	.902	1.325	1.02	51.8	11.9	.41	.45	.96	27.0	.65
1.000	1.000	1.350	1.10	55.2	11.1	.39	.43	.99	25.6	.66

Figure 2.- Velocity-diagram design data.



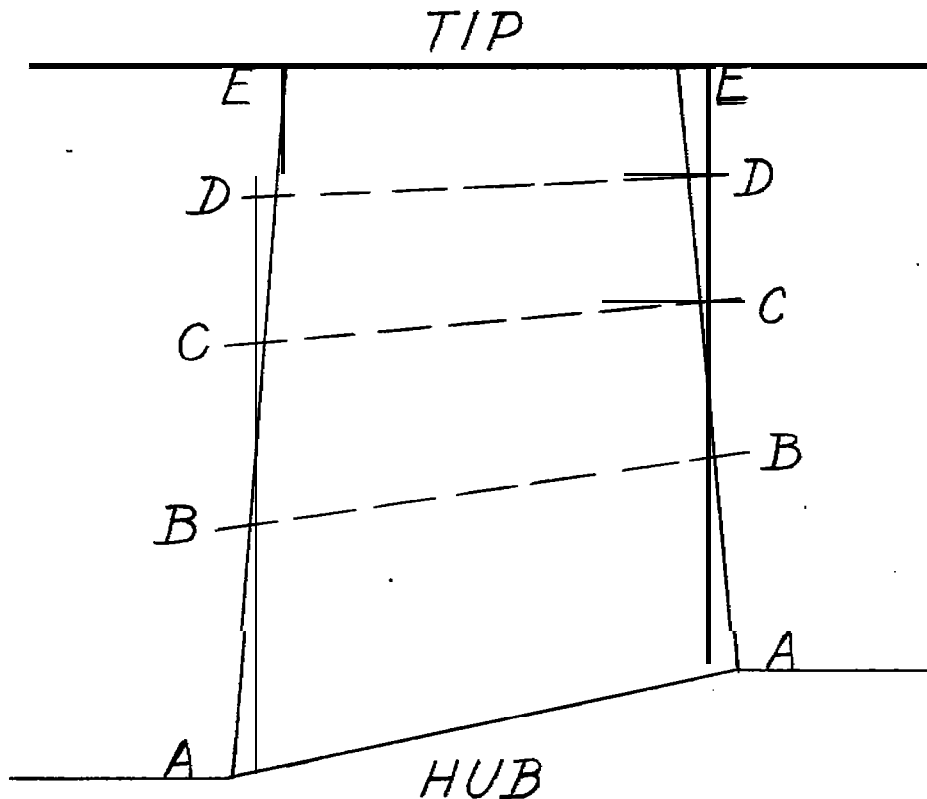
(a) Comparison of T1 and 65-series thickness distributions.

Figure 3.- Thickness-distribution details.



(b) Variation of leading- and trailing-edge radii with blade section thickness for T1 thickness distribution.

Figure 3.- Concluded.



Blade-Section Selection Data

Streamline	$\frac{r_1}{r_t}$	$\frac{r_2}{r_t}$	$\beta_{1R}$ , deg	$\theta_o$ , deg	CL o	$\sigma$	$\frac{t}{c}$	a, deg	$\Delta\alpha$ , deg	$\xi$ , deg
AA	0.350	0.450	27.7	35.4	1.55	1.500	8.0	21.0	2.4	6.7
BB	.585	.646	41.3	22.3	1.14	1.063	6.0	14.6	2.6	26.7
CC	.750	.787	48.1	16.0	.89	.900	5.0	11.5	2.8	36.6
DD	<b>.883</b>	<b>.902</b>	<b>52.3</b>	<b>12.9</b>	<b>.77</b>	<b>.809</b>	<b>4.3</b>	<b>9.9</b>	<b>3.0</b>	<b>42.4</b>
EE	<b>1.000</b>	<b>1.000</b>	<b>55.3</b>	<b>11.3</b>	<b>.70</b>	<b>.750</b>	<b>4.0</b>	<b>8.9</b>	<b>3.2</b>	<b>46.4</b>

Figure 4.- Blade-section selection data. (All angles are based on equivalent velocity diagrams.)

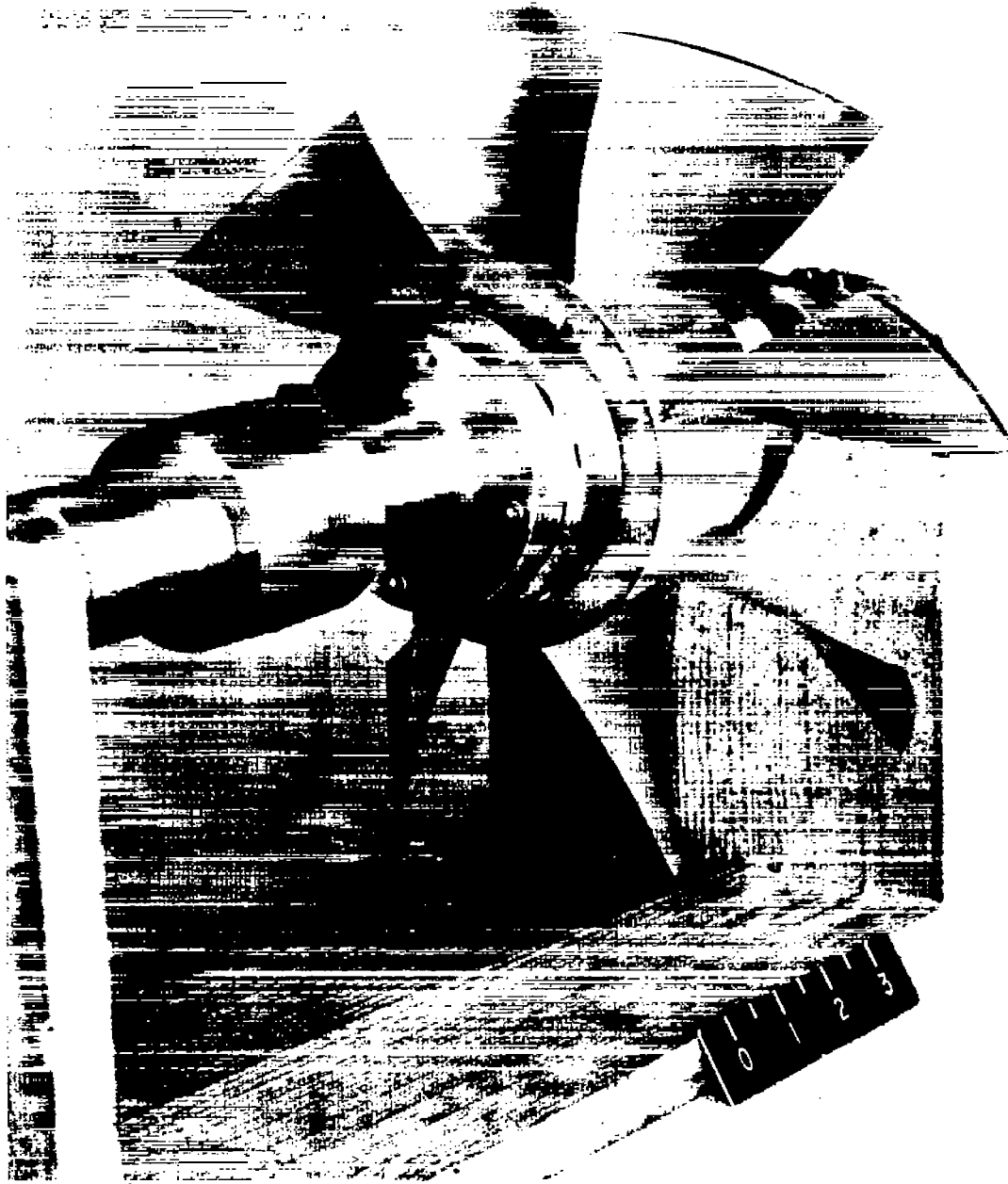
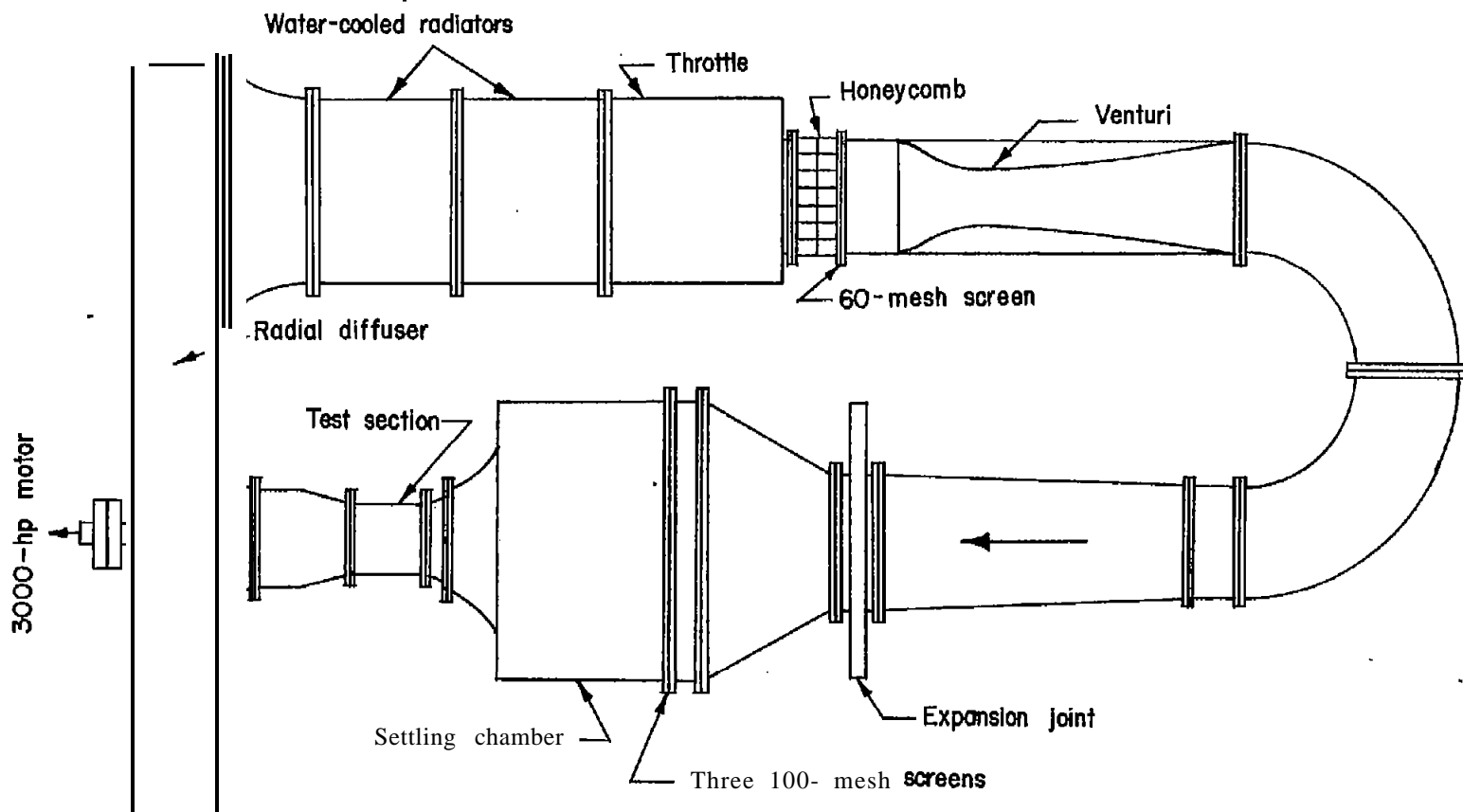
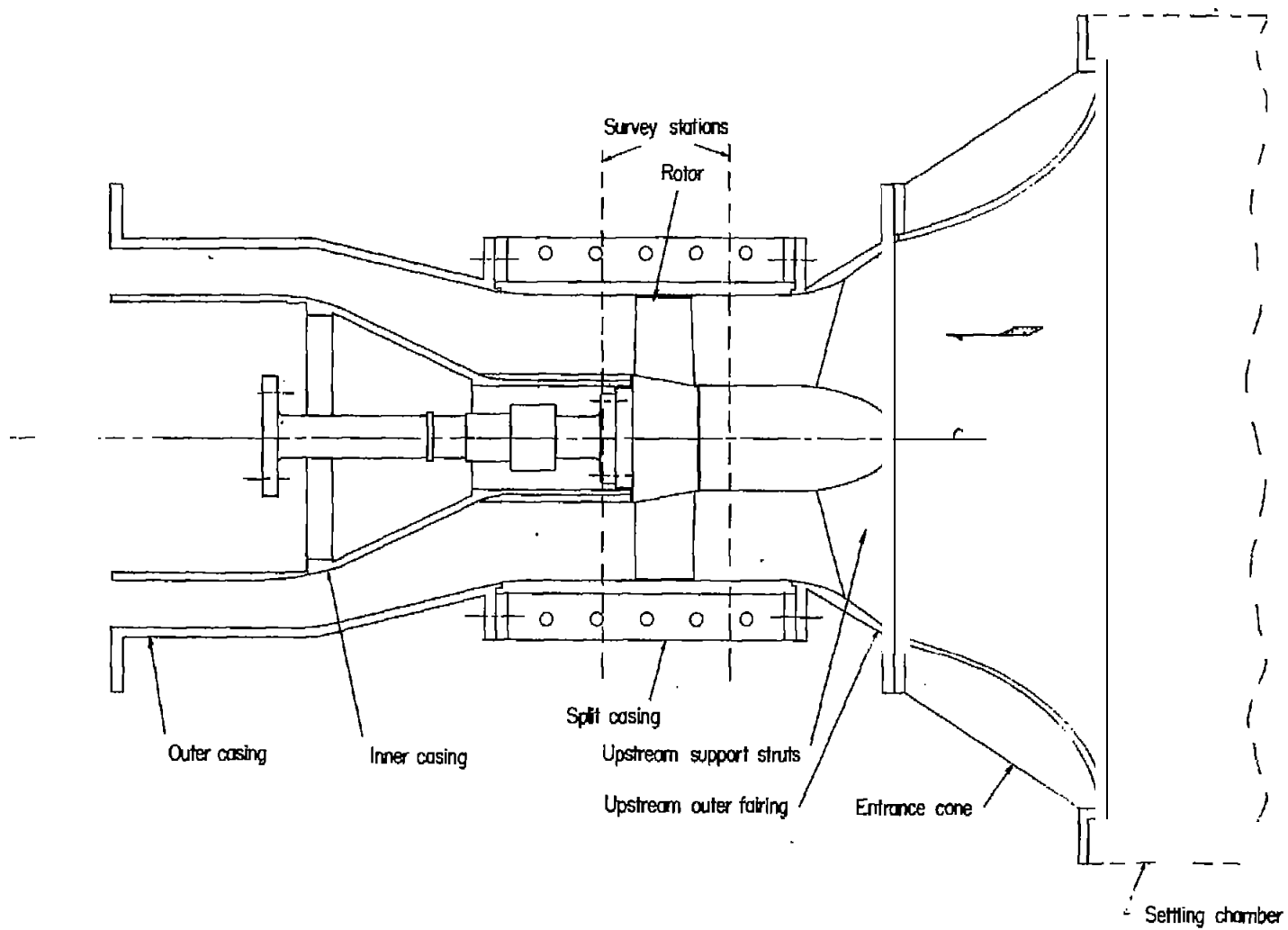


Figure 5.- Photograph of rotor. L-83844



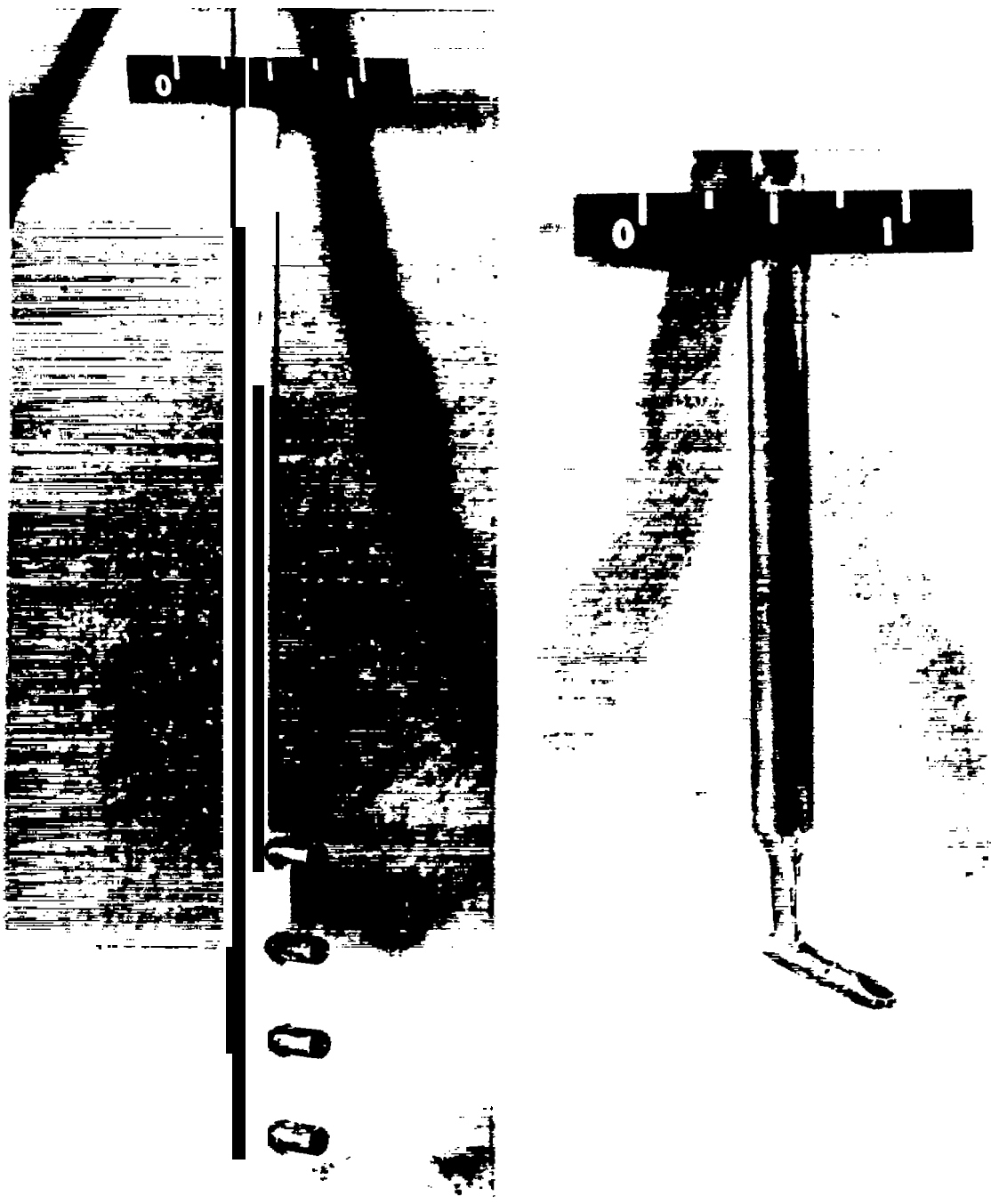
(a) Rig layout.

Figure 6.- Schematic diagram of compressor test installation.



(b) Test-section detail.

Figure 6.- Concluded.

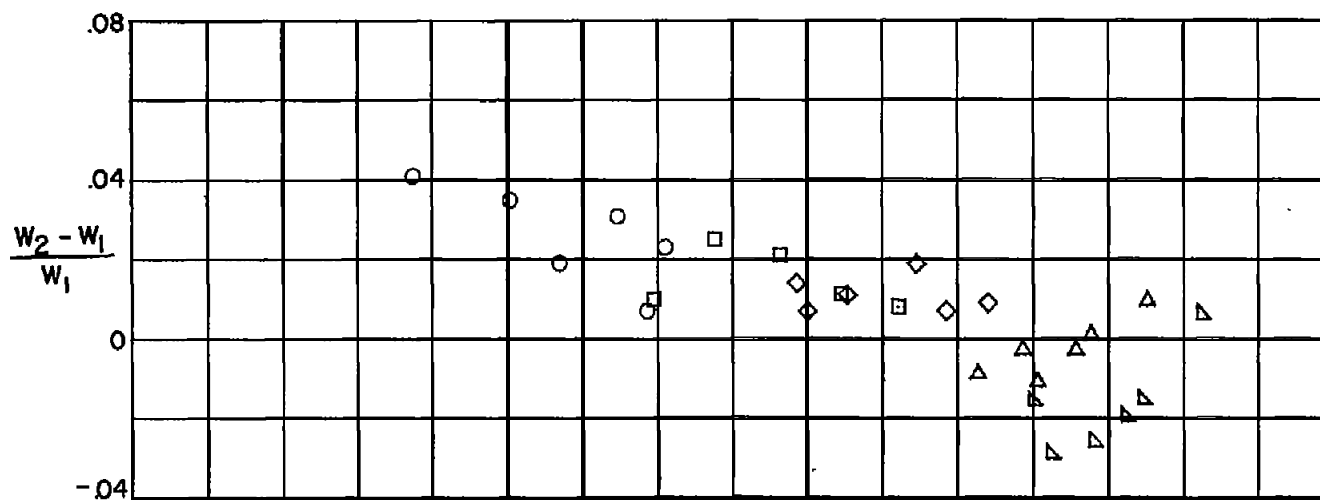


(a) Four bell thermocouple rake.

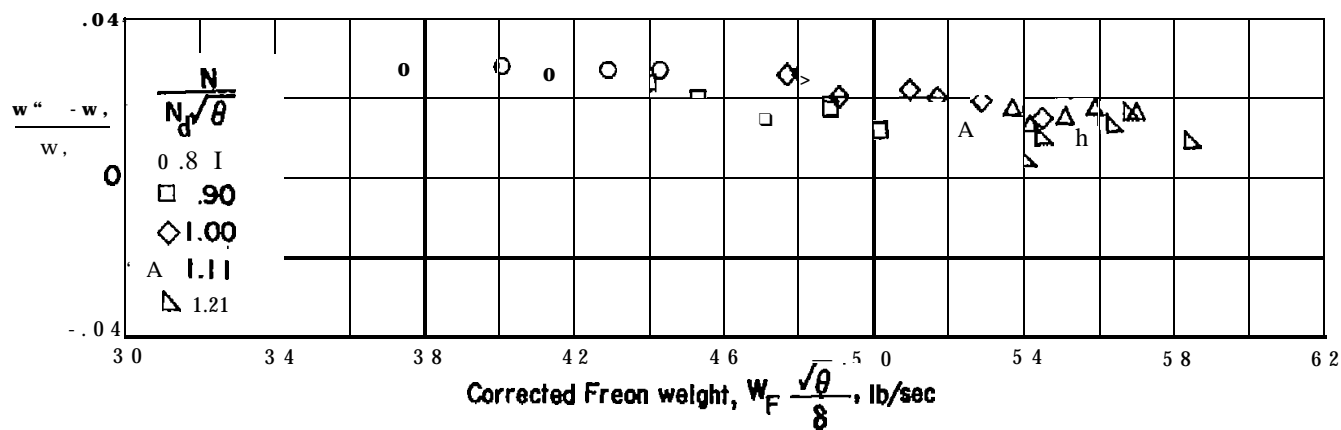
(b) Prism-type survey probe.

**L-87500**

Figure 7.- Instrumentation.

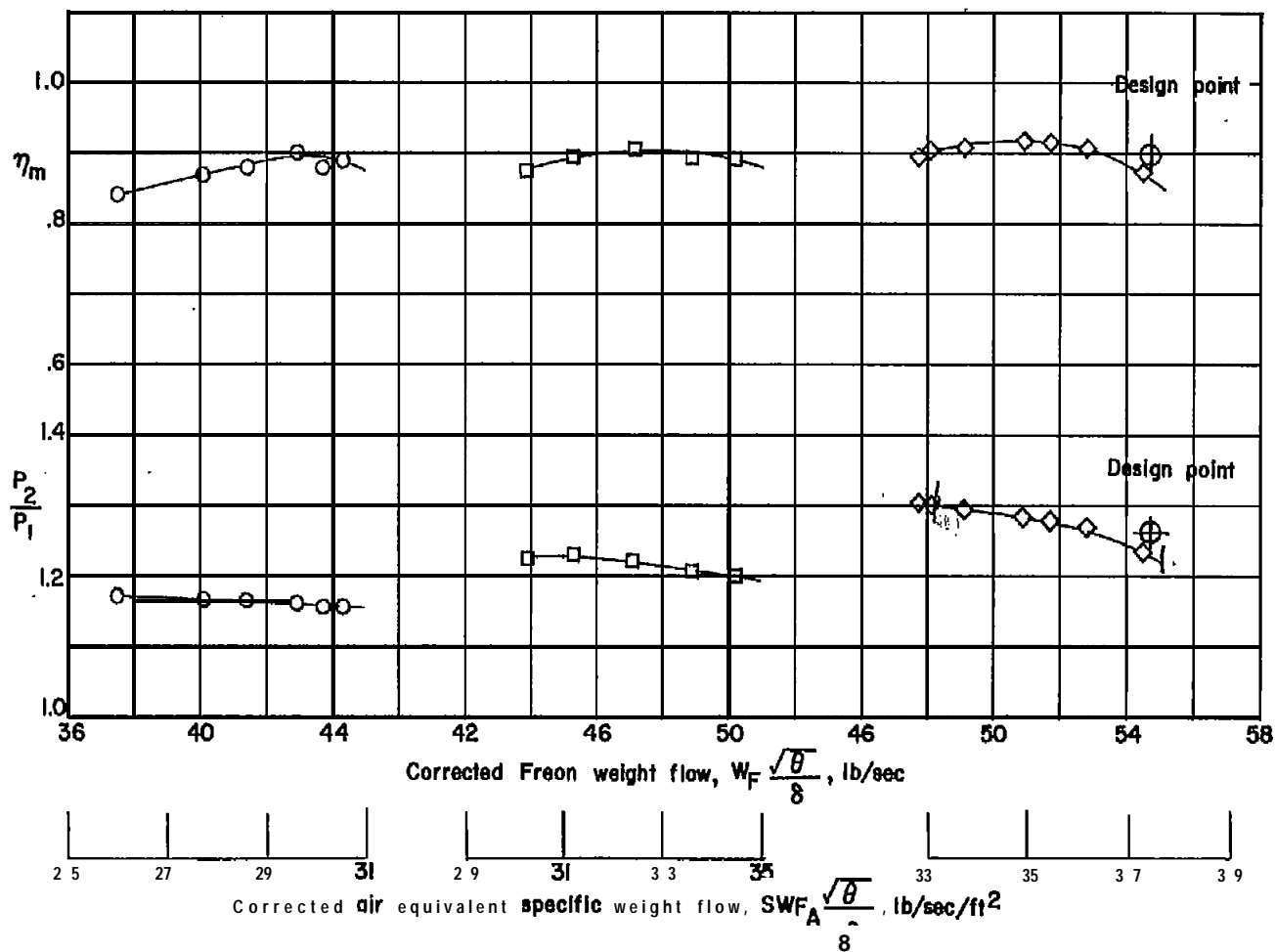


(a) Comparison of upstream and downstream weight flows.



(b) Comparison of upstream and venturi weight flows.

Figure 8.- Comparison of measured weight flows.

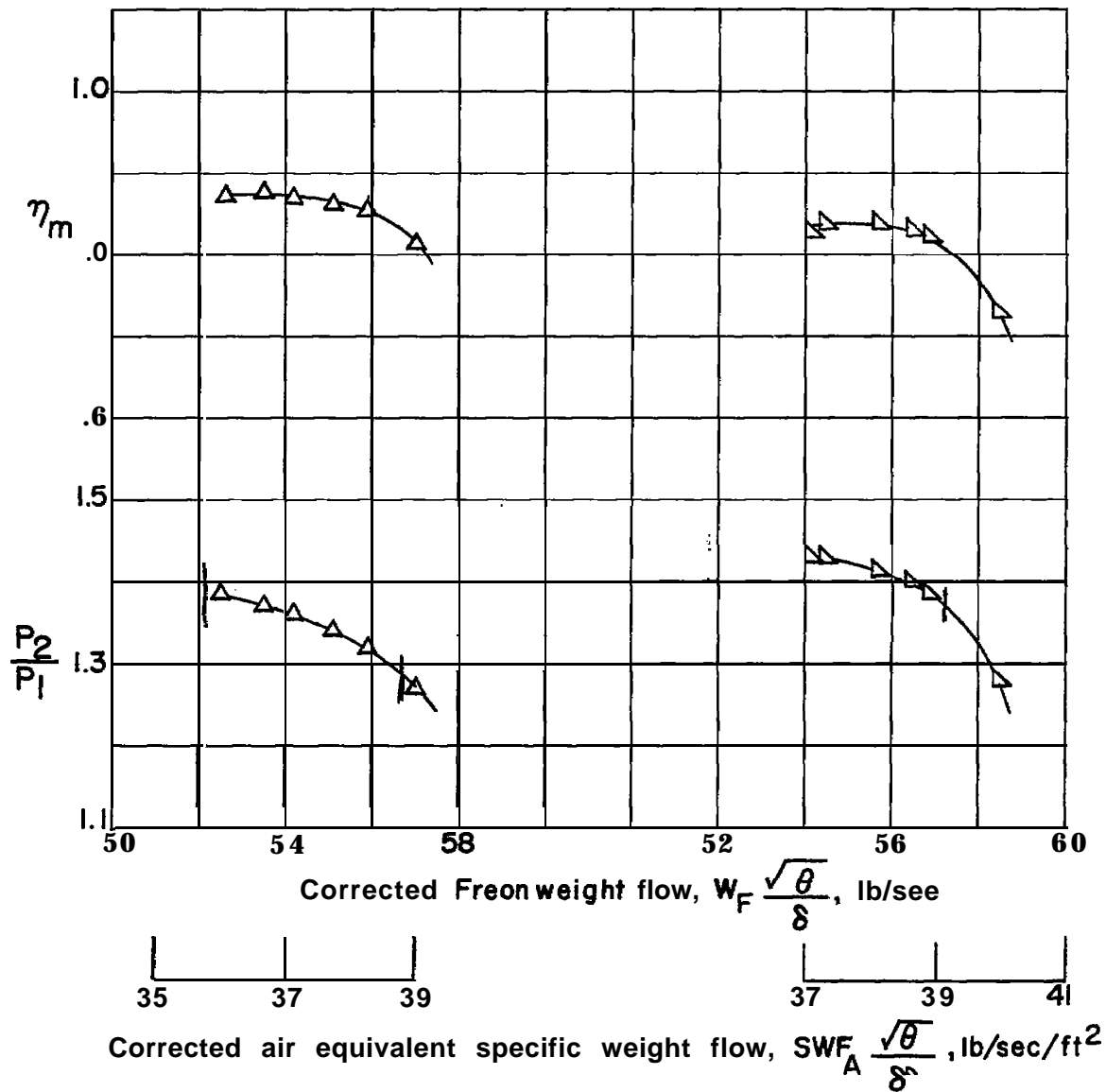


$$(a) \frac{N}{N_d \sqrt{\theta}} = 0.81.$$

$$(b) \frac{N}{N_d \sqrt{\theta}} = 0.90.$$

$$(c) \frac{N}{N_d \sqrt{\theta}} = 1.00.$$

Figure 9.- Rotor performance.



$$(d) \frac{N}{N_d \sqrt{\theta}} = 1.11.$$

$$(e) \frac{N}{N_d \sqrt{\theta}} = 1.21.$$

Figure 9.- Concluded.

NASA Technical Library



31176014371992

CONFIDENTIAL